**DYNAMICS OF MARS AND ORIGIN OF THARSIS.** Lianxing Wen (Dept. of Geosciences, State University of New York at Stony Brook, Stony Brook, NY 11794, Lianxing.Wen@sunysb.edu).

**Introduction:** Whether the topography of Mars is supported by loading of an elastic shell at the surface or by viscous flow in the interior has been controversial [1-9]. On Mars, in particular, because a significant portion of the gravity and topography signals is manifested in the Tharsis province, distinguishing these two mechanisms is also crucial to deciphering origin and formation of Tharsis. Here, I address these issues by separating various components of the topography related to different geological events and studying them through jointly modeling the observed geoid at wavelengths of spherical harmonic degrees $l = 2 – 12$, on the basis of elastic loading and viscous flow.

**Approach:** I construct "residual topography" by excluding the components related to the south-north dichotomy and the major impact basins from the global solutions. I also isolate the topography in the major volcano regions, which I define as "volcano topography". The major volcano regions include the Tharsis province, Elysium and Olympus. I define "dynamic topography" as the topographic contributions related to the deep mantle buoyancy.

If there is no dynamic topography on Mars, the volcano topography should be the manifestation of volcano loading on the outer elastic shell. In this scenario, the residual topography should match the volcano topography plus the flexure effects due to the elastic loading, and the predicted geoid should match the observations, in both amplitude and pattern, at all wavelengths. However, if there is dynamic topography present, the residual topography would represent a combination of the topography related to the volcano load, the flexure effects of the volcano load and dynamic topography. The volcano topography, as defined, is a combination of the topography related to the volcano load (note: different from the volcano topography as defined) and the component due to localization of dynamic topography in the volcano regions. In this scenario, the predicted geoid based on the volcano topography would also be different from the observations. Because the volcano regions can be easily identified and isolated, the above relationships between residual topography, volcano topography and geoid provide a straightforward way to test the volcano loading on an elastic plate and to identify any components of dynamic topography related to deep mantle buoyancy.

**Results:** At the intermediate wavelengths of degrees $l = 4 – 12$, the observed topography of the major volcanoes on Mars, Tharsis, Elysium and Olympus, can account for the residual topography and explain the observed geoid by loading response of a 100-km thick surface elastic layer (Figure 1).

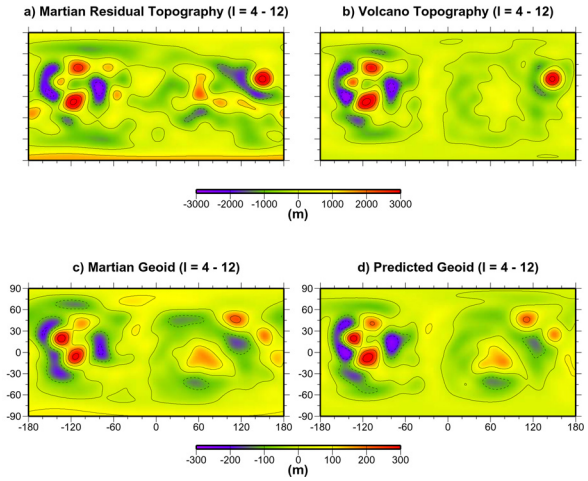


**Figure 1.** Degree $l = 4 -12$ components of a) residual topography, b) volcano topography, c) observed geoid and d) predicted geoid on the basis of an 100-km thick elastic loading model using the volcano topography as boundary condition, with additional contributions from a positive density anomaly in the Utopia basin. Contour intervals are 1200 m in a-b) and 100 m in c-d).

However, at the longest wavelengths of $l = 2 -3$, the volcano topography exhibits considerably less magnitude than the residual topography, and significantly under-predicts geoid on the basis of the elastic loading model inferred from the observations at the intermediate wavelengths of $l = 4 -12$. These mismatches indicate that a significant amount of dynamic topography is present at the longest wavelengths ($l = 2, 3$). The dynamic topography and the portion of the topography related to the volcano load at $l = 2,3$ can be determined on the basis of the residual topography and the volcano topography. Once the topography related to the volcano load is determined, the geoid signals are determined on the basis of elastic loading using the inferred topography related to the volcano load as boundary condition and the parameters of the elastic layer inferred on the basis of the observations at the intermediate wavelengths. The residual geoid is obtained by subtracting the predicted geoid based on the elastic loading from the observations.

I use the inferred dynamic topography and residual geoid to constrain density anomaly in the Martian mantle, assuming an instantaneous viscous flow [10]. The dynamic topography and residual geoid strongly

correlate with the observed geoid, the volcano topography and with each other, indicating that the density buoyancy in the mantle geographically correlates with the major volcanoes. The ratios of dynamic topography and residual geoid observed at $l = 2,3$ further suggest that the low-density anomaly should lie in the deep Martian mantle. Models with a low-density anomaly in the deep lower mantle beneath the Tharsis explain well the dynamic topography and residual geoid at $l = 2,3$ and the lack of them at the intermediate wavelengths. The summation of the predicted dynamic topography and the topography related to the volcano load explains well the residual topography at $l = 2,3$, in both pattern and amplitude. The summation of the predicted geoid on the basis of elastic loading and that based on the density anomaly in the lower mantle also explains well the observations, in both pattern and amplitude. In Figure 2, I present comparisons of topography (Figure 2a,b) and geoid (Figure 2c,d) for a model with a low-density anomaly in the bottom 1050 km of the mantle beneath Tharsis.

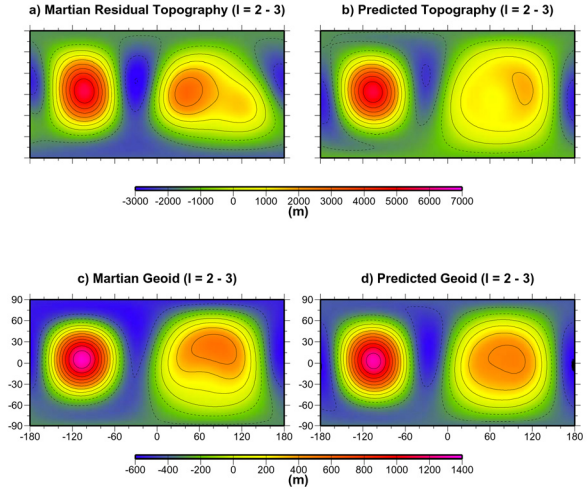


**Figure 2.** Long-wavelength ($l = 2$-$3$) components of a) residual topography, b) predicted total topography, the summation of the topography related to the volcano load and predicted dynamic topography, c) observed geoid and d) predicted total geoid, the summation of the prediction on the basis of the elastic loading using the topography related to the volcano load as boundary condition and that from the density anomaly in the deep mantle. Contour intervals are 800 m in a-b) and 150 m in c-d).

**Dynamics of Mars and a thermochemical plume as origin of Tharsis:** Cartoon in Figure 3a summarizes the present-day dynamics of Mars based on the modeling results of geoid and topography. At present day, an overall low-density anomaly in the lower mantle beneath the Tharsis province induces long-wavelength ($l = 2, 3$) geoid and dynamic topography making the Martian surface (heavy lines) deviating from its hydrostatic figure (dashed lines). The loading of major volcanoes on the surface elastic layer contributes other component of geoid and topography. The combinations of these two mechanisms explain the present-day topography and geoid.

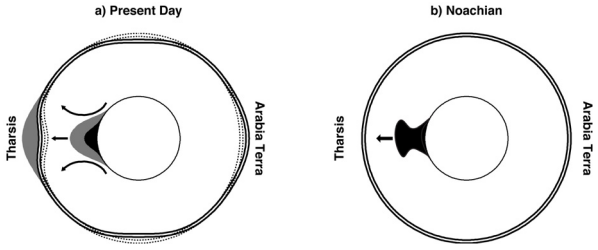


**Figure 3.** Cartoon illustrations of dynamics of the present-day Mars and origin of Tharsis.

The low-density anomaly beneath Tharsis bears extreme analogy to a prominent low-velocity anomaly in the Earth's lower mantle beneath Africa, the so-called "African Anomaly", which is now believed representing a compositional anomaly produced early in the Earth's history [11-12]. I suggest that a thermo-chemical nature of the low-density anomaly beneath Tharsis explains not only its presence, but also the formation, tectonic activities and evolution of Tharsis. At present day, the compositional component (the black portion in Figure 3a), due to its negative density buoyancy, anchors the thermo-chemical anomaly deep in the lower mantle. In Noachian (Figure 3b), a compositional anomaly in the deep Martian mantle beneath Tharsis rapidly focuses mantle flow forming Mars a one thermo-chemical plume planet (black object). The eruption of the thermo-chemical plume head forms the Tharsis province and the remaining portion of the compositional anomaly survives through present day, providing source to the long-lived, recurring volcanoes in the Tharsis province throughout the Martian history.

**References:** [1] Solomon, S. C. & Head, J. R. (1982) *JGR, 87,* 9755-9774. [2] Phillips, R. J. et al. (2001) *Science, 291*, 2587-2591. [3] McGovern, P. J. et al. (2002) *JGR, 107*, doi:10.1029/2002JE001854. [4] Carr, M. H. (1973) *JGR, 78,* 4049-4062. [5] Kiefer, W. S. & Hager, B. H. (1989) *LPI Tech. Report, 89-04,* 48-50. [6] Harder H. & Christensen, U. (1996) *Nature, 380,* 507-509. [7] Banerdt W. B. & Golombek, M.P. (2000) *LPS, 31,* Abstract#2038. [8] Turcotte, D. L. et al. (2002) *JGR, 107*,5091, doi:10.1029/2001JE001594. [9] Zhong, S. & Roberts, J. H. (2003) *EPSL, 214,* 1-9. [10] Wen, L. & Anderson, D. L. (1997) *JGR, 102,* 24,639-24,654. [11] Wen, L. et al. (2001*) EPSL, 189,* 141-153. [12] Wen, L. (2006) *EPSL, 246,* 138-148.